Winter 12-2016

Analysis of drift effects on the tokamak power scrape-off width using SOLPS-ITER

E. T. Meier
College of William and Mary, emeier@wm.edu

R. J. Goldston

E. G. Kaveeva

M. A. Makowski

S. Mordijck

See next page for additional authors

Recommended Citation

Meier, E. T.; Goldston, R. J.; Kaveeva, E. G.; Makowski, M. A.; Mordijck, S.; Rozhansky, V. A.; Senichenkov, I. Yu; and Voskoboynikov, S. P., Analysis of drift effects on the tokamak power scrape-off width using SOLPS-ITER (2016). *PLASMA PHYSICS AND CONTROLLED FUSION*, 58(12). 10.1088/0741-3335/58/12/125012

PAPER

Analysis of drift effects on the tokamak power scrape-off width using SOLPS-ITER

To cite this article: E T Meier *et al* 2016 *Plasma Phys. Control. Fusion* **58** 125012

Analysis of drift effects on the tokamak power scrape-off width using SOLPS-ITER

E.T. Meier,[1, a)] R.J. Goldston,[2] E.G. Kaveeva,[3] M.A Makowski,[4] S. Mordijck,[1] V.A. Rozhansky,[3] I. Yu. Senichenkov,[3] and S.P. Voskoboynikov[3]

[1)] *College of William and Mary, Williamsburg, VA 23187, USA*

[2)] *Princeton Plasma Physics Laboratory, P.O. Box 451, Princeton, NJ 08543, USA*

[3)] *Peter the Great St. Petersburg Polytechnic University, Polytechnicheskaya 29, 195251 St. Petersburg, Russia*

[4)] *Lawrence Livermore National Laboratory, Livermore, CA 94550, USA*

(Dated: 15 September 2016)

SOLPS-ITER, a comprehensive 2D scrape-off layer modeling package, is used to examine the physical mechanisms that set the scrape-off width (λ_q) for inter-ELM power exhaust. Guided by Goldston's heuristic drift (HD) model, which shows remarkable quantitative agreement with experimental data, this research examines drift effects on λ_q in a DIII-D H-mode magnetic equilibrium. As a numerical expedient, a low target recycling coefficient of 0.9 is used in the simulations, resulting in outer target plasma that is sheath limited instead of conduction limited as in the experiment. Scrape-off layer (SOL) particle diffusivity (D_{SOL}) is scanned from 1 to 0.1 m^2/s. Across this diffusivity range, outer divertor heat flux is dominated by a narrow (~3-4 mm when mapped to the outer midplane) electron convection channel associated with thermoelectric current through the SOL from outer to inner divertor. An order-unity up-down ion pressure asymmetry allows net ion drift flux across the separatrix, facilitated by an artificial mechanism that mimics the anomalous electron transport required for overall ambipolarity in the HD model. At D_{SOL} = 0.1 m^2/s, the density fall-off length is similar to the electron temperature fall-off length, as predicted by the HD model and as seen experimentally. This research represents a step toward a deeper understanding of the power scrape-off width, and serves as a basis for extending fluid modeling to more experimentally relevant, high-collisionality regimes.

Keywords: power scrape-off width, heuristic drift model, plasma drifts, SOLPS-ITER

[a)] Electronic mail: emeier@wm.edu

I. INTRODUCTION

Power crossing the last closed flux surface in diverted tokamaks is exhausted along open field lines to divertor targets through a channel characterized, during the quasi-steady inter-ELM period, by a power scrape-off width (λ_q). The smaller this width, the more challenging it is to sufficiently dissipate the power such that the heat flux at the plasma facing components is tolerable. Not only does a more narrow channel naturally result in higher heat flux, but the smaller associated plasma volume corresponds to less radiation for a given density, temperature, and impurity content. The tight connection between λ_q and peak steady-state heat flux has motivated a concerted effort to predict λ_q in ITER. Experimentally, the focus has been on regression analysis of tokamak parameters such as size, aspect ratio, toroidal and poloidal magnetic field (B_{tor} and B_{pol}), culminating in the work of Eich et al.[1,2], which shows, in short, that λ_q scales as $B_{pol}^{-1,2}$, and projects that λ_q in ITER will be $\approx$ 1 mm — significantly less than the previously assumed 3.6 mm. Modeling using the SOLPS code[3] has addressed implications of $\lambda_{q,ITER} \approx$ 1 mm. Though the modeling focused on carbon divertor targets (ITER now plans to use exclusively tungsten) without impurity injection, the basic results would likely hold for scenarios with tungsten divertor targets and impurity injection: The operational window is dramatically narrowed, and the achievable power gain (Q) is reduced[4].

Thus, there is a strong impetus to understand the physical basis of the $\lambda_q \propto B_{pol}^{-1,2}$ scaling. Goldston has proposed an heuristic drift (HD) model[5] that provides excellent agreement with experimental data in terms of both absolute value and scalings[6]. The conceptual basis of the HD model is depicted in Fig. 1, and can be summarized as follows. Vertical grad B and curv B drifts, together referred to as magnetic drifts, drive ion flux from the core into the scrape-off layer (SOL) in the lower-outer quadrant. (In the equilibrum used for this research, shown in Fig. 1, due to high triangularity, magnetic drifts in the lower-inner quadrant have only a small component directed across flux surfaces, so this discussion will focus on the outer SOL; an anlagous mechanism could operate in the inner SOL for equilibria with lower triangularity.) In the outer SOL, the Pfirsch-Schlüter (P-S) circuit is disrupted by flows moving to the outer target at approximately half of the sound speed ($c_s/2$). From the lower-outer quadrant, some of cross-separatrix ion flux returns to the top via the usual P-S path, but some is entrained in the divertor flow. The crux of the HD model is that competition between the radial ion flux, driven at the magnetic drift speed, and the $c_s/2$ divertor flow sets the density channel width, characterized by the gradient scale length (L_n). The

HD model then assumes that radial turbulent electron thermal transport fills the density channel, but cannot transport energy beyond the channel simply because such energy transport vanishes in a vacuum. As a result, $\lambda_q \propto L_n$. Experimental analysis of the ASDEX Upgrade (AUG) tokamak shows that the inter-ELM ratio of the electron density gradient and electron temperature gradient near the separatrix, $\eta_e \equiv L_{ne}/L_{Te}$, is approximately constant for a database of ~~34~~ 36 shots (all with attached divertor conditions, and with a limited range of B_{tor}), with $\eta_e \approx 1.4$ [7]. The correlation of L_{ne} and L_{Te} seems to support the HD model, and also suggests that critical gradient turbulence could be playing a role. Good agreement is also found between the HD model and near-SOL λ_q measurements on several tokamaks in limiter configuration [6,8–10]. The fact that the HD model reproduces experimental scalings and closely agrees with a variety of experimental data motivates exploration of the proposed physics mechanisms through detailed SOL modeling.

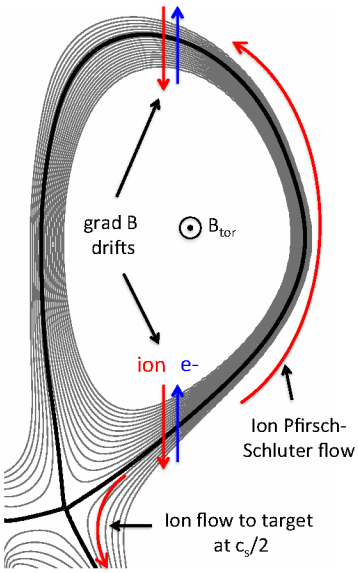

FIG. 1. Schematic of the interrupted Pfirsch-Schlüter SOL flow pattern that is central to the HD model.

Fluid modeling with drifts has covered a variety of topics, such as in-out asymmetries[11], SOL parallel flows[12,13], and net cross-separatrix fluxes[14], but has not been used to address the physics basis of λ_q. The results presented below, in which SOLPS-ITER is used to analyze low-collisionality plasmas with 90% target recycling and sheath-limited outer target conditions, represent the first dedicated fluid modeling analysis of drift effects on λ_q. Modeling setup is presented in Section II. Results and discussion are given in Sections III and IV. Conclusions are drawn in Section V. The primary goal of the research is to assess the ability of laminar fluid edge modeling (using SOLPS-ITER, in particular) to capture the underlying mechanisms of the HD model. To the extent

that the modeling does not reproduce HD physics, a natural secondary goal is to understand why not and whether improvements to the modeling should be considered.

II. MODELING SETUP

Modeling is done with the SOLPS-ITER code package[15,16] (added Ref. [16]), which employs the plasma drift physics capability of SOLPS5.2[17,18]. The fluid neutral model of SOLPS-ITER is used in favor of the EIRENE Monte Carlo neutral code[19], which is also available. The fluid neutral model is not as quantitatively accurate, but is more computationally manageable than EIRENE. When looking for "zeroth-order" drift effects, this tradeoff is beneficial. No comparison of fluid vs. kinetic neutrals has been made in this modeling. For simplicity, impurity species are omitted, and pure deuterium plasma is assumed.

DIII-D discharge 158139 at 2650 ms is used as a subject. This deuterium H-mode discharge had 10 MW neutral beam input power, $B_{tor} = -2$ T (giving downward ion ∇B drift), and plasma current $I_p = 1.5$ MA. Results presented below are ~~for~~ from simulations that all use ~~a~~ the orthogonal computational grid shown in Fig. 2 with 36 poloidal × 18 radial cells ~~, shown in Fig. 2~~. Using higher resolutions (54×27 and 72×36), qualitatively similar results are obtained, but numerical convergence at very low SOL particle diffusivities (see below) has not been possible due to difficulty resolving gradients in the electrostatic potential that exist near the separatrix, especially in the divertor region. The core boundary is located 4.5 cm inside the outer midplane separatrix at normalized flux $\psi_n = 0.85$. In all simulations, density at the core boundary is fixed at 4.5×10^{19} m^{-3}, and core boundary temperatures are also fixed, to $T_e = T_i = 500$ eV. As mentioned in the introduction, a relatively low 90% target recycling is used; experimental recycling levels are much higher, near 100%. (The divertor cryopump, located near $Z = -1.4$ m and $R = 1.4$ m in Fig. 2, was active in this discharge, but is not specifically modeled here.) There are two reasons that low recycling is used: first, the physics picture is simplified by minimizing neutral effects in the SOL; second, the high-recycling case has proven to be more numerically challenging.

Particle diffusivity in most of the core region is 1 m^2/s, while SOL diffusivity is set by a parameter, D_{SOL}. From a radial position 5 mm inside the outer midplane separatrix to the separatrix, particle diffusivity transitions linearly from 1 m^2/s to D_{SOL} as shown in the inset of Fig. 3. This radial diffusivity profile is applied uniformly in the poloidal direction, except in the divertor region, where the SOL value is multiplied by 5, as shown in Fig. 3. Ion and electron cross-field thermal

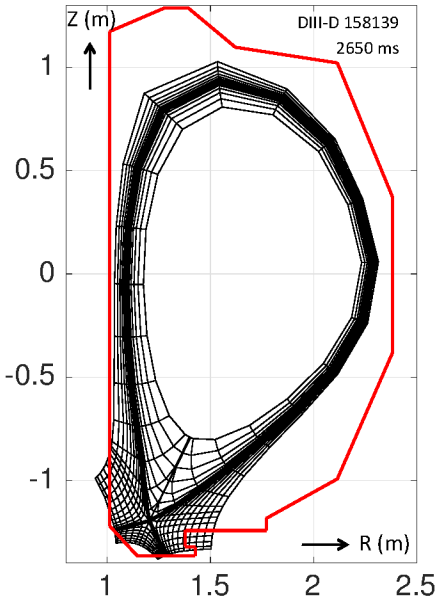

FIG. 2. Orthogonal grid based on EFIT magnetic reconstruction of DIII-D discharge 158139 at 2650 ms.

diffusivities are 1 m^2/s everywhere in the domain, except in the divertor region, where they are 5 m^2/s. Cross-field momentum diffusivity is 1 m^2/s everywhere. For classical fluxes, flux limits are applied: for neutral diffusion, flux is limited to the thermal flux; electron and ion parallel heat fluxes are limited to 30% and 60%, respectively, of the thermal fluxes. Sensitivity of solutions to these flux limits is not considered here, but should not qualitatively affect the results.

Three different plasma drift cases are considered: no drifts; full drifts (i.e., including curvature B, grad B, and $E \times B$ drifts); and only magnetic drifts (i.e., excluding $E \times B$ drifts). The various drifts are turned on or off in the entire domain, rather than in selected spatial zones. For each case, a baseline simulation is established with $D_{SOL} = 1$ m^2/s. D_{SOL} is then scanned from 1 to 0.1 m^2/s as descibed in Section III.

Following standard practice, power scrape-off widths are determined based on the outer target heat flux profile, due to relatively high peak steady-state heat flux there compared to the inner target. The Eich fitting approach[1] is used to determine λ_q^{Eich}, which represents the power scrape-off width at the outer divertor target, mapped along flux surfaces to the outer midplane.

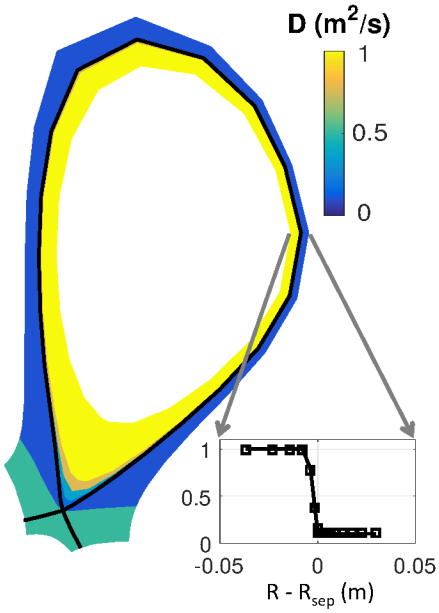

FIG. 3. 2D particle diffusivity profile with $D_{SOL} = 0.1$ m^2/s. Inset shows radial profile at the outer midplane.

III. RESULTS

A. Scan of SOL particle diffusivity

For each simulation in the D_{SOL} scans, Fig. 4(a) shows density and electron temperature gradient scale lengths (L_n and L_{Te}), and Fig. 4(b) shows λ_q^{Eich}. For all cases (no drifts, full drifts, and only magnetic drifts), L_n is significantly larger than L_{Te}, except near $D_{SOL} = 0.1$ m^2/s. Values of L_n for the full-drift and magnetic-only cases are larger than the corresponding L_n values for the no-drift case across the range of D_{SOL}. As $D_{SOL} \to 0$, L_n in the cases with magnetic drifts approaches a value twice as large as in the no-drift case. At small D_{SOL}, the simulated scale lengths match observed values reasonably well, though the observed scale lengths have not been formally quantified. Consider, for example, the full-drift case at $D_{SOL} = 0.1$ m^2/s. In that case, L_n and L_{Te} are within ~50% of the observed values. Two-point models for collisional SOL conditions indicate $\lambda_q = 2/7 L_{Te}$ [7,20]; thus, the experimental $\lambda_q = 2.0$ mm, corresponds roughly with the simulated $L_{Te} = 5.8$ mm. At the outer midplane separatrix, simulated density is 2.5×10^{19} m^{-3}, vs. an experimental value of 2.0×10^{19} m^{-3}, while the simulated electron temperature is 120 eV vs. an experimental value near 80 eV. As will be discussed below, the large difference in separatrix temperature causes simulated results to deviate from experimental reality; useful insights will still be obtained by analyzing the simulations.

For simulations without drifts, λ_q^{Eich} is sensitive to D_{SOL}, varying from 5.9 mm at 1 m^2/s to

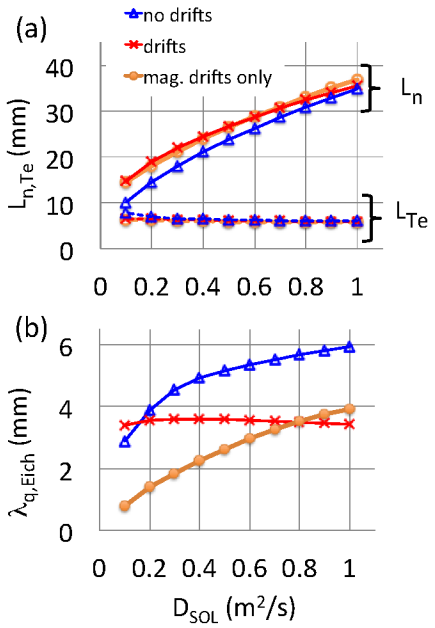

FIG. 4. Panel (a): Gradient length scales in scans of SOL particle diffusivity (D_{SOL}). Gradient scale lengths for density (L_n; solid lines) and electron temperature (L_{Te}; dashed lines) are calculated at the outer midplane separatrix. Panel (b): λ_q found using Eich fitting.

2.9 mm at 0.1 m^2/s. Simulations with full drifts have significantly smaller λ_q^{Eich} at the highest D_{SOL} = 1 m^2/s — 3.4 mm vs. 5.9 mm in the no-drift case — and λ_q^{Eich} remains relatively constant over the range of D_{SOL} explored. As elaborated in Section IV, this insensitivity of λ_q^{Eich} to D_{SOL}, though intriguing, is apparently due to a coincidental cancellation of effects. In the scan with only magnetic drifts, λ_q^{Eich} is reduced with decreasing D_{SOL}, similar to the no-drift case.

Fig. 5 gives the outer target heat flux profile for the full-drift simulation with D_{SOL} = 0.1 m^2/s, along with the experimental data from DIII-D. Eich-style fits are also shown. Experimental and simulated peak heat fluxes are quite different, with the simulated value more than three times larger than the measured one, while simulated and measured λ_q are closer: 3.2 mm and 2.0 mm, respectively. For comparison, the predictions of the Eich regression and the HD model are 2.2 mm and 2.0 mm, respectively. (Regression #14 is used from Eich et al.[2], and pure deuterium plasma is assumed for the HD prediction.) Also indicated in the figure are the Gaussian spreading factors, S. The smaller S in the simulation reflects the relatively low simulated collisionality; as discussed above, simulated target recycling is only 90%, in contrast with the near 100% recycling from the saturated DIII-D targets. The difference in simulated and measured peak heat flux is largely due

to the absence of impurity radiation in these simulations,[1] which allows unrealistically high total power deposition on the divertor targets.

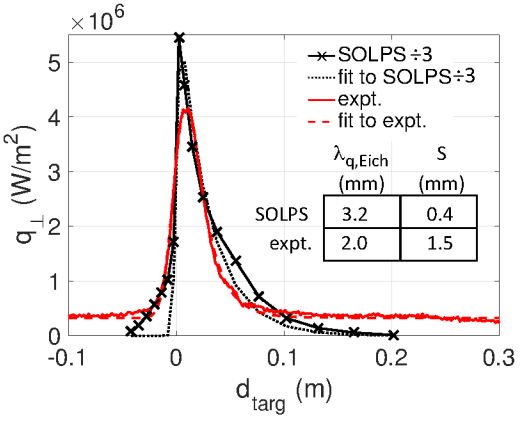

FIG. 5. Deposited outer target heat flux vs. distance along target from separatrix (d_{targ}). Results of the full-drift simulation at D_{SOL} = 0.1 m^2/s (labeled "SOLPS"; divided by 3 to facilitate visual comparison) and from corresponding DIII-D heat flux measurement (labeled "expt.") are shown, along with Eich-style fits. Positive d_{targ} indicates the SOL, while negative indicates the private flux region.

B. Drift-induced thermoelectric effect

Fig. 6(a) and (c) compare the electrostatic potential (ϕ) to $3T_e$ (where T_e is in eV) for inner and outer targets, respectively, in the full-drift simulation with D_{SOL} = 0.1 m^2/s. Targets are assumed to be grounded with ϕ = 0 V. Sheath analysis[20] shows that, for a pure deuterium plasma without secondary electron emission, when $\phi = 3T_e$ ($\equiv \phi_{float}$), there is no current through the sheath, i.e., the plasma "floats." When inner and outer target temperatures differ, the so-called thermoelectric current[20,22,23] is carried from the hotter target to the colder target. In the case depicted in Fig. 6, the inner target is in a conduction-limited regime, with strike point $T_e \approx 25$ eV and $n_e \approx 10^{20}$ m^{-3}, compared to the outer target which is in a sheath-limited regime with strike point $T_e \approx 100$ eV and and $n_e \approx 10^{19}$ m^{-3}. At the inner target, ϕ rises above ϕ_{float} such that the sheath favors ion transmission, and the current to the target is approximately given by the ion saturation current. Radial currents, even in the SOL, are small, so currents to the inner and outer targets must be similar. The inner target collects a large ion current due to the high density there, while the ion

[1] Typically in DIII-D, impurity radiation dominates the total radiation—see, for example, work by Porter et al.[21]. To capture realistic radiation in DIII-D, not only must carbon must be included in the modeling, but high target recycling must be used to achieve low SOL temperatures, near 10 eV, at which carbon becomes an efficient radiator.

current to the outer target is small. Thus, ϕ at the outer target is suppressed relative to ϕ_{float} such that electrons pass easily through the sheath to give the required current. Fig. 6(b) and (d) show target heat fluxes. The effect of the suppressed ϕ on the outer target heat flux is clear: the heat flux is dominated by a non-conductive electron component associated with this thermoelectric current. The negative electron thermal conduction from the outer target to the plasma is ~~due to a shortcoming of the energy boundary condition in SOLPS-ITER~~ surprising from a sheath physics standpoint and, arguably, should not be allowed by the electron energy boundary condition; it is a minor component of heat flux, however, and can be ignored for the purposes of this analysis. The basic role of the thermoelectric current is consistent with a qualitative analytical model by Rozhansky et al.[24], though SOLPS-ITER solutions presented here violate some of the assumptions of[24], and the role found here is stronger than predicted by that model. In the no-drift case, the inner and outer target temperatures are similar, and the thermoelectric effect is minimal.

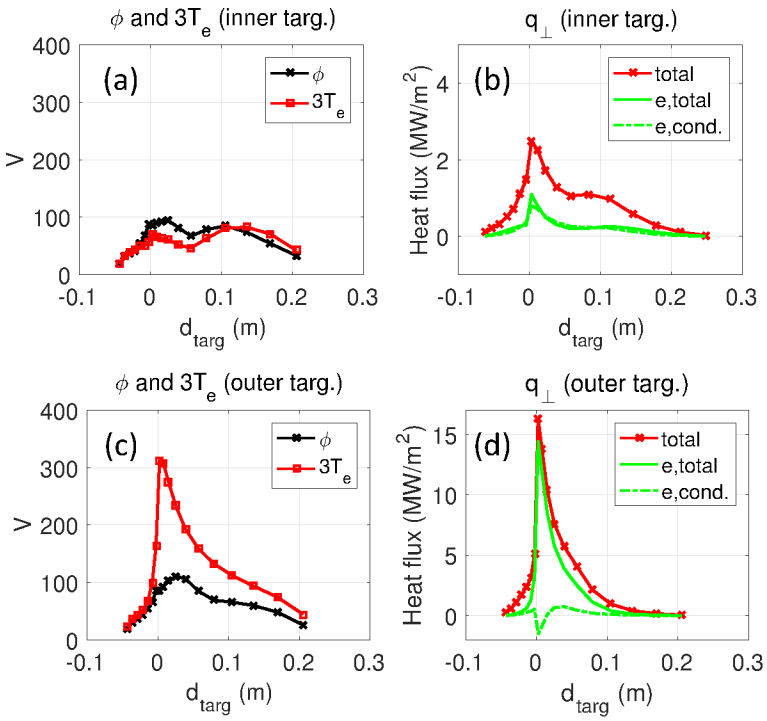

FIG. 6. Electrostatic potentials and heat fluxes in full-drift simulation at D_{SOL} = 0.1 m^2/s. Panels (a) and (c) show the sheath potential (ϕ) and floating potential ($3T_e$) at the inner and outer targets as a function of target position. Total heat flux ("total"), total electron heat flux ("e, total"), and the conducted components of electron heat flux are shown in panels (b) and (d) for inner and outer targets.

C. Up-down ion pressure asymmetry and net flux due to magnetic drifts

Ion particle flux behavior is revealed by the streamline plots in Fig. 7. In steady state, the equation governing density evolution is $\nabla\cdot(n\mathbf{V}_i) = S_i$, where n is the density, $\mathbf{V}_i$ is the ion velocity, and S_i is the ion source rate. Streamlines follow vectors of momentum, $n\mathbf{V}_i$, and their divergence is determined by S_i. In Fig. 7, streamlines are launched at each of the cells immediately inside the separatrix and follow ion momentum vectors for 5 m or until termination at the domain boundary. In the no-drift case, streamlines trace ion momentum vectors both forward and backward from the launch points to provide streamlines in the core region. In the other cases, streamlines are drawn only in the forward direction. Without drifts [panel (a)], a flow separatrix occurs at the outer midplane. With full drifts [panel (b)], the flow separatrix occurs in the lower outer quadrant. As in the HD model, the outboard P-S flow pattern is interrupted by flow to the divertor. In the lower-outer quadrant, within 20 cm of the X-point, particles pass through the separatrix (carried mostly by magnetic drifts), and eventually reach the outer target. Closer to the outer midplane, particles crossing the separatrix in the lower-outer quadrant return in the upper-outer quadrant, following the classical P-S pattern. From the separatrix indicated in the figure, the flow is directed toward the inner target without reversing directions; in a plasma with lower triangularity, an inboard P-S pattern might appear, with associated flow reversals. With only magnetic drifts [panel (c)], the outboard P-S pattern is similar to the full-drift case, but the fluxes in the inner and outer divertor regions are different.

Based on the outboard P-S pattern in the full-drift case, up-down asymmetry might be expected. As shown in Fig. 8(a), an ion pressure asymmetry is observed in the simulations. The asymmetry factor rises as D_{SOL} is reduced, with the factor peaking at 1.50 at $D_{SOL} = 0.1$ m^2/s; as magnetic flux becomes a major source of ions in the SOL, the asymmetry is enhanced. Fig. 8(b) reveals a strong density asymmetry and very little asymmetry in T_i.

A detailed accounting of cross-separatrix fluxes is given in Fig. 9 for the full-drift simulation with $D_{SOL} = 0.1$ m^2/s. The SOL particle diffusivity is sufficiently low that net magnetic fluxes are comparable to the anomalous particle flux. The role of radial (across flux surfaces) flux due to perpendicular viscosity ($\Gamma_r^{\eta\perp}$) is pivotal, though not entirely physical. This flux is associated with a radial drift due to perpendicular (within flux surfaces) viscous force, i.e.,

$$\Gamma_r^{\eta\perp} \equiv nV_r^{\eta\perp} = \frac{F_\perp^\eta}{e|\mathbf{B}|} \quad , \quad F_\perp^\eta \propto \frac{\partial}{\partial r}\eta_\perp \frac{\partial}{\partial r} V_\perp^{drift},$$

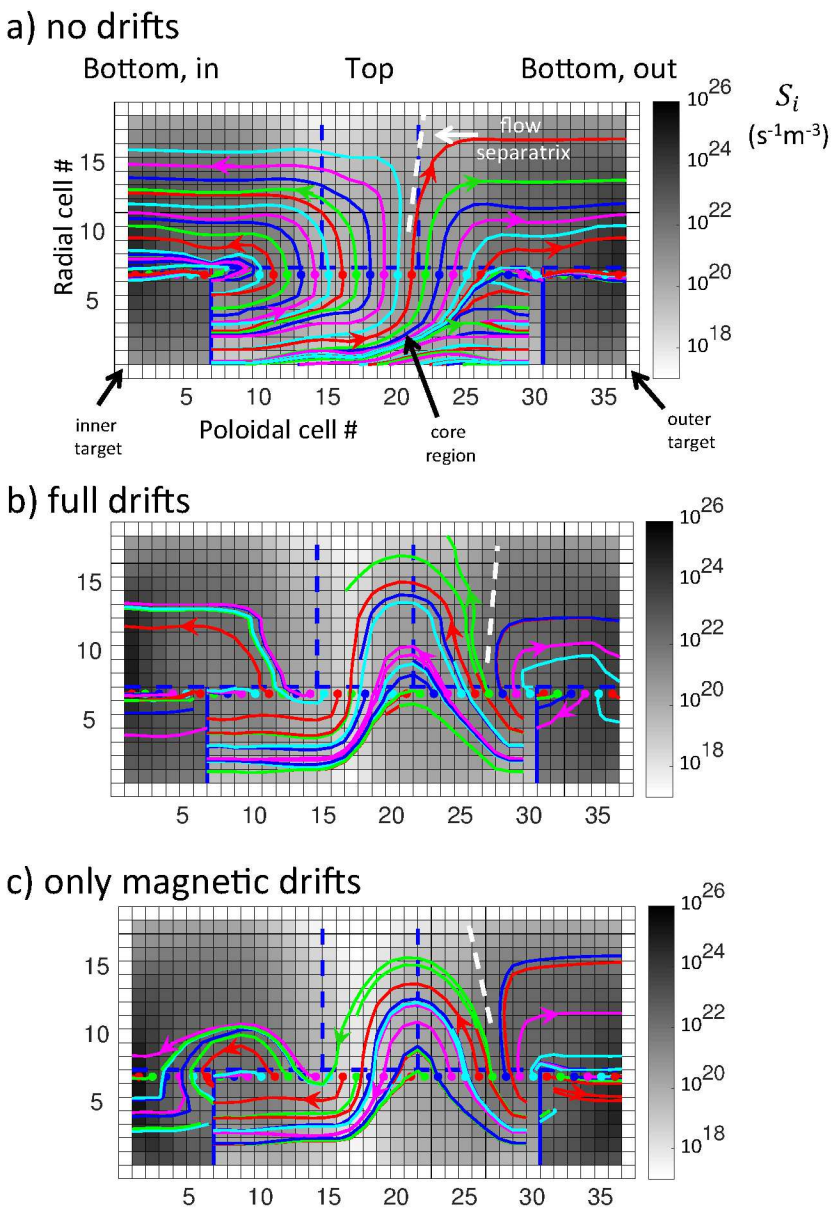

FIG. 7. Streamlines of ion flux for simulations with D_{SOL} = 0.1 m^2/s and (a) no drifts (b) full drifts and (c) only magnetic drifts. Streamline traces are launched and traced as described in the main text. Alternating colors are used for clarity, and arrowheads indicate flow direction. The ion particle source (S_i) is shown in grayscale. Logical space is used instead of physical space such that cells each occupy squares of identical size. The separatrix, and inner and outer midplanes are indicated with dashed lines. Solid lines separate the private flux regions from the core region; physically, of course, the two private flux regions are contiguous, and the core region is periodic.

where $V_{\perp}^{drift}$ includes electric and diamagnetic perpendicular drift speeds. Only the dominant part

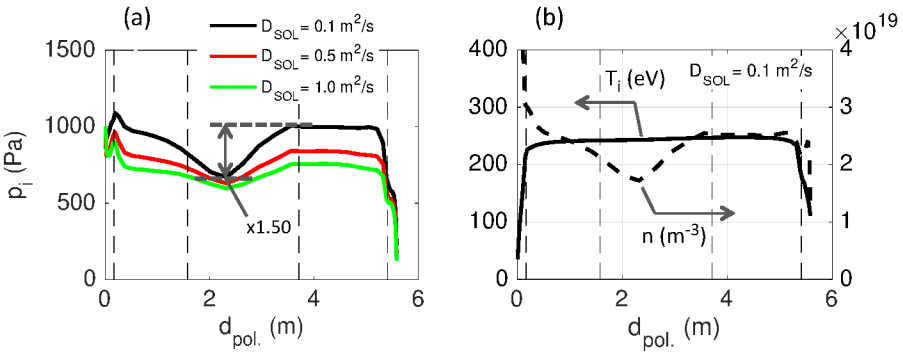

FIG. 8. Ion pressure, temperature and density at separatrix as a function of poloidal position from inner target to outer target. Panel (a): ion pressure profiles for three values of D_{SOL}. The highest up-down ion pressure asymmetry factor is 1.50 for D_{SOL} = 0.1 m^2/s. Panel (b): ion temperature and density profiles for D_{SOL} = 0.1 m^2/s. Density at the inner target goes off-scale, reaching a peak value of 1.6 $\times 10^{20}$ m^{-3}. Vertical dashed lines indicate locations of, from left to right, the X-point, inner midplane, outer midplane, and (again) the X-point.

of the volumetric force $F_{\perp}^{\eta}$ is shown here, and only this part is included in the model — see[17,18] for details. Though $\Gamma_r^{\eta\perp}$ is physically an ion flux, numerically, it is included as a component of the electron flux, with reversed sign such that the current is unchanged. This allows a significant non-diffusive ion flux, mostly due to magnetic drifts. If, however, $\Gamma_r^{\eta\perp}$ were included in the ion flux, the net non-diffusive flux would be near zero. This is an important point that is further discussed in Section IV.

IV. DISCUSSION

At low D_{SOL}, modeling with magnetic drifts (i.e., the full-drift case and the magnetic-only case) gives $L_n \approx L_{Te}$ as $D_{SOL} \to 0$. As mentioned in the introduction, this connection of scale lengths underlies the HD theory[5]; to see this result in SOLPS-ITER modeling is encouraging. Moreover, at the lowest D_{SOL} (0.1 m^2/s), L_n is a factor of two larger when magnetic drifts are included, lending further credence to the HD concept that magnetic drifts set the density channel width.

As shown in Fig. 4, L_n is significantly larger than L_{Te} across most of the D_{SOL} range, and η_e is as high as 7 at the highest D_{SOL}. This result contrasts strongly with the recent AUG results, which find $\eta_e \approx 1.4$ for a variety of discharges. In the HD theory, it is assumed that cross-field transport is sufficient to fill the plasma density channel. In this modeling, cross-field thermal

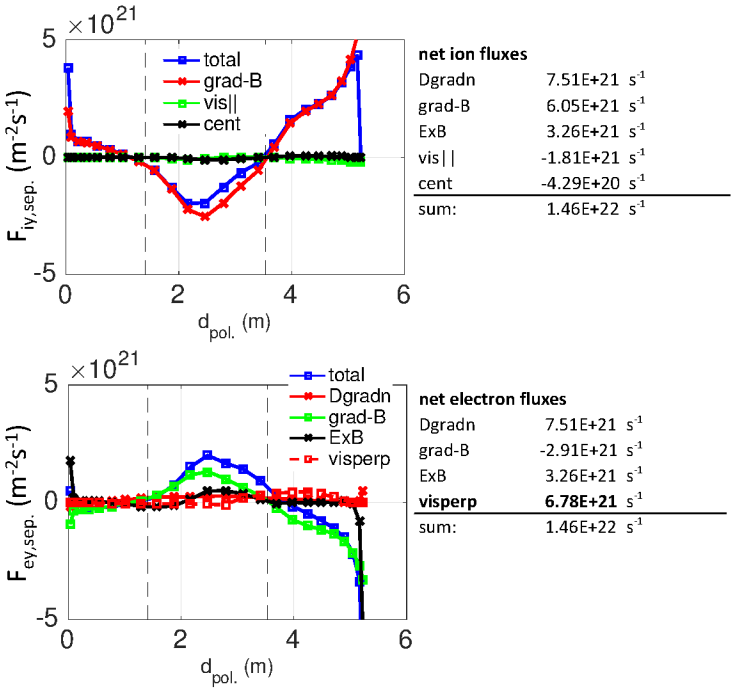

FIG. 9. Cross-separatrix fluxes of ions (top) and electrons (bottom) in a full-drift case with D_{SOL} = 0.1 m^2/s, as a function of poloidal distance ($d_{pol.}$) moving clockwise, starting and ending at the X-point. Fluxes from the core to the SOL are positive. Anomalous particle diffusion ("Dgradn") and $E \times B$ flux are the same for both species and are only shown in the plot of electron fluxes. The "grad-B" flux represents grad B and curv B drifts. Also shown are drifts due to parallel viscosity ("vis||"), the centrifugal effect ("cent") perpendicular viscosity ("visperp"). Fluxes with net values less than 10^{20} s^{-1} are not shown.

diffusivity set to a "typical" value, 1 m^2/s — a value that is clearly too low to produce $\eta_e \approx 1.4$. Physically, temperature gradients that are significantly steeper than density gradients could drive critical gradient, drift-wave turbulence as suggested by Sun et. al[7] and by Neuhauser et al. in earlier AUG experimental work[25]. A connection between η_e and drift-wave turbulence has been suggested theoretically, and parametrizations of such turbulent transport in terms of gradient scale lengths have been proposed[26]. In future SOLPS-ITER analysis of λ_q scaling, implementation of such parameterizations could prove insightful.

The insensitivity of λ_q to D_{SOL} in the full-drift case is apparently due a complicated interplay of effects. Most likely, such insensitivity would not prove to be a robust simulation result across different SOL and divertor collisionalities. A complete explanation of the observed insensitivity is ~~beyond the scope of this discussion~~ elusive, but it is worth noting the following two effects, which

seem to play leading roles: First, there is an cross-field "convection" of energy that is directly proportional to D_{SOL} (due to an effective velocity, $v_D = D_{SOL}\nabla n/n$), so that lower D_{SOL} tends to reduce λ_q. Second, the region of low T_e at the inner target becomes broader as D_{SOL} is reduced, so that the channel of thermoelectric current (see Section III B) is wider. The broadening of the low T_e region, in turn, seems related to a general reduction of separatrix temperature (and associated increase in density) as D_{SOL} is reduced, and an increased radial $E \times B$ drift flux. As D_{SOL} is reduced, this latter effect seems to counterbalance the first one, resulting in a nearly constant λ_q. In the HD picture, at sufficiently low D_{SOL} (say 0.1 m^2/s or less), one would expect insensitivity of λ_q to D_{SOL}, with magnetic drifts determining the particle behavior in the SOL, but insensitivity across a wide range of D_{SOL} is unexpected. Again, the insensitivity is probably specific to the conditions simulated here, and would not hold in general.

As noted in Section III A, with only magnetic drifts, at $D_{SOL} = 1$ m^2/s, λ_q is similar to the full-drift case, but varies strongly with D_{SOL} like the no-drift case. At $D_{SOL} = 1$ m^2/s, strongly peaked non-conductive electron power deposition exists at the outer target despite little current at the inner target — radial SOL currents are strong enough to enable this feature. Similar to the no-drift case, however, λ_q trends lower with decreasing D_{SOL}. Apparently, without $E\times B$ drifts, the thermoelectric current channel does not broaden as discussed above (the second "effect" related to the insensitivity of λ_q to D_{SOL} in the full-drift case). A related point is that, in the case with only magnetic drifts, the inner strike point is cooler than the outer strike point (approximately 20 eV vs. 100 eV), similar to the full-drift case, despite the absence of $E \times B$ drifts that tend to cool the inner target. This appears to be due to an ion flow separatrix as found in the full-drift case, yielding upward flow at the outer midplane, which may enhance particle transport to the inner target. In contrast, in the no-drift case inner and outer strike point temperatures are similar (near 50 eV) such that the thermoelectric effect is absent. In general, it appears that the low-recycling, sheath-limited conditions simulated here magnify the thermoelectric effect and $E \times B$ drifts, and thus modify λ_q scaling behavior, simply because temperatures and temperature gradients tend to be high, especially at the outer target.

Simulations with D_{SOL} lower than 0.1 m^2/s were not numerically achievable. Although further research is necessary to identify with certainty the cause of the numerical problems, strong gradients in electric field, particularly in E_r near the X-point and in divertor legs along the separatrix, seem to be responsible for poor convergence due to strongly sheared $E \times B$ flows. Gradients in E_r tend to grow with increasing resolution, suggesting that the numerical scheme, as it stands, is

not convergent at resolutions that are realistically attainable. Presently, the electrostatic potential is smoothed by means of an anomalous electric current that is proportional to $\nabla\phi$. Additional smoothing that can be localized near the regions of extreme electric field shear would be worth exploring in future work. For example, a current proportional to $\nabla\mathbf{E}\cdot\nabla\phi$ could be implemented.

In the HD model, magnetic drifts dominate the ion particle flux across the separatrix, while anomalous particle transport is relatively small. As discussed in[27], cross-separatrix electron drift fluxes (due to $E\times B$ and diamagnetic drifts) locally cancel for a Boltzmann electron distribution, $n_e \sim \exp(e\phi/T_e)$; this condition is well satisfied in the simulations presented here, judging by the near cancellation of net $E\times B$ and magnetic fluxes as tabulated in Fig. 9. With vanishing anomalous particle diffusion, this cancellation yields small net electron flux, since anomalous diffusion, $E\times B$ drift, and magnetic drift are the only components of electron particle flux included in the standard Braginskii-based model of SOLPS-ITER. Overall ambipolarity requires the same small net ion flux. Thus, to permit the significant net particle fluxes seen experimentally in H-mode plasmas ($\sim 5\times10^{21}$ s^{-1} in DIII-D[28]), the HD model requires net cross-separatrix electron flux from some additional mechanism. Numerically, as mentioned in Section III C, the ion drift flux due to perpendicular viscosity ($\Gamma_r^{\eta\perp}$) is carried in the electron channel in these SOLPS-ITER simulations. For the purposes of this initial exploration of HD physics, the presence of such artificial electron transport is useful, enabling the up-down asymmetric ion pressure discussed in Section III C. In future work, physically plausible mechanisms, e.g., electron transport along stochastic field lines[6], which is implemented as an option in SOLPS-ITER[29], can be considered.

V. CONCLUSIONS

SOLPS-ITER has been used in an initial exploration of the HD model for power scrape-off width scaling in a low-recycling scenario with sheath-limited outer target plasma. Simulations at low SOL particle diffusivity, $D_{SOL}\approx 0.1$ m^2/s, achieve a regime relevant to the HD model, with comparable density and temperature gradient length scales at the outer midplane separatrix. In addition, several aspects of the results are investigated in detail:

- Full-drift simulations show an intriguing insensitivity of λ_q to D_{SOL}, whereas no-drift simulations show the expected reduction of λ_q with D_{SOL}. The insensitivity in the full-drift case is attributed to a nontrivial dependence of particle transport on SOL diffusivity and magnetic and $E\times B$ drifts.

- Thermoelectric current establishes a narrow non-conductive electron heat flux feature that dominates the outer target power deposition footprint.
- An up-down asymmetry in ion pressure enables net cross-separatrix ion magnetic flux with magnitude consistent with experimental results for H-mode plasmas.

Following this preliminary fluid modeling research, future work should aim to advance SOLPS-ITER analysis of the HD model by closely matching experimental conditions and improving model assumptions. For example, the work presented here could be extended to high-collisionality (conduction-limited) SOL conditions with impurities and associated radiation. Improved numerical smoothing of electrostatic potential and associated electric fields may be necessary near the X-point and in the divertor legs along the separatrix. Ambipolarity of net cross-separatrix particle flow should be established using mechanisms that are fully physical, and grounded in experimental data, if possible. Parameterization of cross-field thermal transport could be modified to account for experimental evidence of a critical gradient ratio $\eta_e \approx 1.4$ above which turbulent transport might be enhanced. Finally, scans of relevant plasma parameters, such as device size, poloidal and toroidal magnetic field, would be valuable.

VI. ACKNOWLEDGMENTS

This work has been performed under U.S. Department of Energy Contract DE-SC0010434.

REFERENCES

[1]T. Eich *et al.*, Phys. Rev. Letters **107**, 215001 (2011).

[2]T. Eich *et al.*, Nucl. Fusion **53**, 093031 (2013).

[3]R. Schneider *et al.*, Contrib. Plasma Phys. **46**, 3 (2006).

[4]A. Kukushkin *et al.*, J. Nucl. Mater. **438**, S203 (2013).

[5]R. J. Goldston, Nucl. Fusion **52**, 013009 (2012).

[6]R. J. Goldston, J. Nucl. Mater. **463**, 397 (2015).

[7]H. J. Sun *et al.*, Plasma Phys. Control. Fusion **57**, 125011 (2015).

[8]M. Kocan *et al.*, Nucl. Fusion **55**, 033019 (2015).

[9]R. Dejarnac *et al.*, J. Nucl. Mater. **463**, 381 (2015).

[10]S. Wiesen *et al.*, J. Nucl. Mater. **463**, 385 (2015).

[11]G. D. Porter *et al.*, Phys. Plasmas **17**, 112501 (2010).

[12]P. A. Molchanov *et al.*, Plasma Phys. Control. Fusion **50**, 115010 (2008).

[13]V. A. Rozhansky *et al.*, J. Nucl. Mater. **363**, 605 (2007).

[14]A. V. Chankin and D. P. Coster, J. Nucl. Mater. **463**, 498 (2015).

[15]S. Wiesen *et al.*, J. Nucl. Mater. **463**, 480 (2015).

[16]X. Bonnin *et al.*, Plasma Fusion Res. **11**, 1403102 (2016).

[17]V. A. Rozhansky *et al.*, Nucl. Fusion **41**, 387 (2001).

[18]V. A. Rozhansky *et al.*, Nucl. Fusion **49**, 025007 (2009).

[19]D. Reiter, M. Baelmans, and P. Börner, Fusion Sci. Technol. **47**, 172 (2005).

[20]P. C. Stangeby, *The plasma boundary of magnetic fusion devices* (IOP publishing Ltd., 2000).

[21]G. D. Porter *et al.*, Phys. Plasmas **7**, 3663 (2000).

[22]P. J. Harbour, Contrib. Plasma Phys. **28**, 417 (1988).

[23]G. M. Staebler and F. L. Hinton, Nucl. Fusion **29**, 1820 (1989).

[24]V. A. Rozhansky *et al.*, in Proceedings of the 38th European Physical Society Conference on Plasma Physics, 2011 (Strasbourg, France) , P4.074.

[25]J. Neuhauser *et al.*, Plasma Phys. Control. Fusion **44**, 855 (2002).

[26]Y. C. Lee *et al.*, Phys. Fluids. **30**, 1331 (1987).

[27]A. V. Chankin and D. P. Coster, J. Nucl. Mater. **438**, 463 (2013).

[28]G. D. Porter and DIII-D Team, Phys. Plasmas **5**, 4311 (1998).

[29]V. A. Rozhansky *et al.*, Nucl. Fusion **50**, 034005 (2010).